



Development of Highly Stable Ni-Al₂O₃ Catalysts for CO Methanation

Zhifeng Qin^{1,4,5} · Hongyan Ban¹ · Xiaoyue Wang¹ · Zhibin Wang¹ · Yanxia Niu² · Ying Yao³ · Jun Ren¹ · Liping Chang¹ · Maoqian Miao¹ · Kechang Xie¹ · Congming Li¹

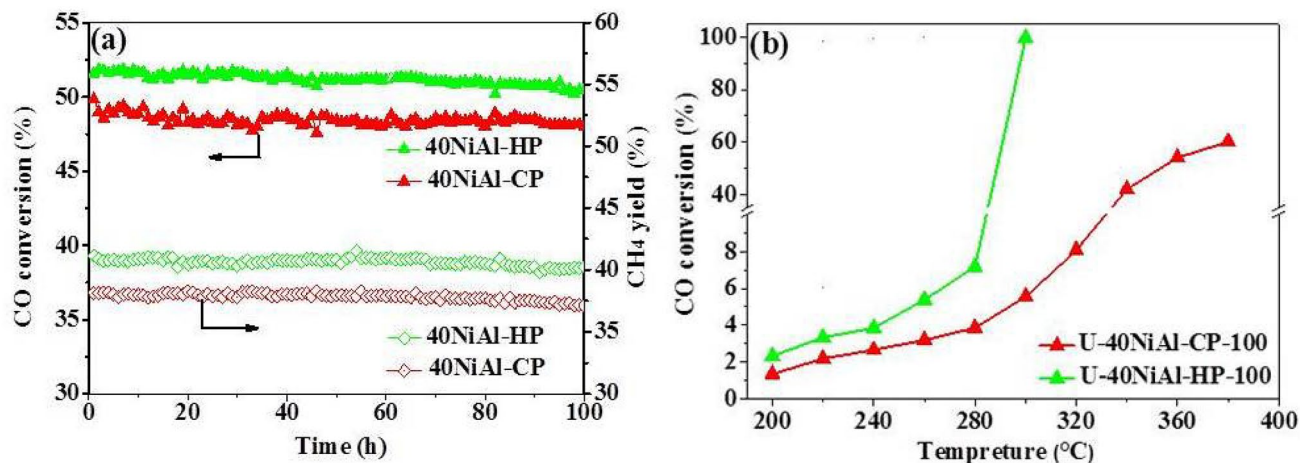
Received: 12 August 2020 / Accepted: 1 December 2020

© The Author(s), under exclusive licence to Springer Science+Business Media, LLC part of Springer Nature 2021

Abstract

A series of Ni-Al₂O₃ catalysts with attractive catalytic activity and thermal stability have been developed via a facile hydrolysis-precipitation technique (xNiAl-HP, x representing the weight percentage of NiO). Based on the high nickel active surface area, good dispersion of NiO and high content of α - and β_1 -type NiO, outstanding CO conversion (99%) and CH₄ yield (96%) can be achieved over 40NiAl-HP under mild conditions [T = 220 °C, P = 1.0 MPa, and WHSV = 20,000 mL/(g·h)]. The reaction-sintering at high temperature (800 °C) evolves through: (a) the migration of nickel crystals, (b) the phase transformation from γ - to θ - and then to α -Al₂O₃, and (c) the agglomeration of catalyst particles. The 40NiAl-HP catalyst could still maintain CO conversion over 99% at 300 °C after being used at 800 °C for 100 h. Herein, the high catalytic activity, good sintering resistance and noble-metal-/promoter-free nature might make 40NiAl-HP a competitive candidate for industrial methanation.

Graphic Abstract



Keywords CO methanation · Ni-Al₂O₃ · Hydrolysis-precipitation · Low temperature · Sintering resistance

Supplementary Information The online version of this article (<https://doi.org/10.1007/s10562-020-03486-4>) contains supplementary material, which is available to authorized users.

✉ Zhifeng Qin
qinzhifeng@tyut.edu.cn

✉ Congming Li
licongming0523@163.com

Extended author information available on the last page of the article

1 Introduction

Natural gas (NG), as a kind of clean energy with a high heating value (37.26 – 28.10 MJ/m³) and a high energy efficiency, has been widely applied in many fields such as chemical and power industries, transportation fuel and residential use etc. [1]. In view of the increased demand of natural gas, the development of synthetic natural gas (SNG) is of vital

importance in some regions of the world [2]. Especially in China, the strategy of “Coal to Natural Gas” has been highly developed in recent years due to the primary energy structure of China (70% coal, 20% oil and 4% natural gas) [3]. To reduce the dependence on coal and oil, the government aims at increasing the proportion of natural gas in the total energy system [4, 5]. The production of SNG from coal/biomass/coke oven gas is in line not only with the tendency towards a clean utilization of coal, but with the goal of changing the primary energy mix [6–8].

In recent years, carbon monoxide (CO) methanation, has been regarded as a competitive technology to afford SNG from syngas. The catalysts based on group VIII metals (*e.g.* Ni, Rh, Ru, Pd and Pt) have been widely developed for CO methanation [6–17]; among them, Ni-Al₂O₃ catalysts have attracted much attention due to the superior activity in methanation and relatively low cost [8–11, 18–26]. However, active Ni component is easily to be sintering following quick deactivation, and Al₂O₃ commonly suffer from unsatisfactory thermal stability [20–24]. Considering the strongly exothermic nature of CO methanation, it is critical to develop catalysts with high activity and good stability under harsh conditions. Very recently, MCR-2X catalyst was reported to maintained the relative high activity for CO methanation beyond two years at an exit temperature of 675 °C, it seems important to improve the sintering resistance of catalysts under series conditions [11, 26].

So far, numerous researches have focused on the enhancement of the catalytic activity and thermal stability of Ni-Al₂O₃ catalysts via introducing promoters (*e.g.* La, Na, Mg, W) [16, 17, 24–26] and varying preparation methods (*e.g.* impregnation, solution combustion, co-precipitation, homogeneous precipitation) [16–26]. Considering the low cost of common Al₂O₃ support, it is promising to develop a facile preparation technique for Ni-Al₂O₃ catalysts that exhibits superior catalytic activity and thermal stability rather than introducing special promoters.

Herein, a series of Ni-Al₂O₃ catalysts with high catalytic activity and good sintering resistance in CO methanation were synthesized by hydrolysis-precipitation method. In view of the fact that few reports have focused on the implications of a reaction temperature that is considerably higher than that commonly adopted in industrial applications (650 °C), the catalytic performance at low temperature (220 °C) and lifetime test at harsh temperature (800 °C) of the prepared Ni-Al₂O₃ catalysts have been investigated. The correlation of the catalytic activity and thermal stability with the textural structures was also concerned and discussed in detail.

2 Experimental

2.1 Catalyst Preparation

2.1.1 Preparation of Ni-Al₂O₃ Catalysts by Hydrolysis-Precipitation

Typically, known quality of nickel nitrate hexahydrate [Ni(NO₃)₂, 0.21 mol/L] and sodium aluminate [NaAlO₂, 0.90 mol/L] were dissolved into 100 mL of deionized water separately under vigorous stirring. The Ni(NO₃)₂ solution was added into the aluminum precursor solution at a rate of 2 mL/min. The suspension was stirred by a magnetic stirrer and its pH was maintained at about 10. The mixture was aged for 12 h at 70 °C, and the resultant white precipitate was collected via filtration. After being washed with water (30 mL × 3), the obtained light green powder was dried at 100 °C for 12 h and then calcined at 450 °C for 2 h under N₂ atmosphere in a tubular furnace. The Ni-Al₂O₃ catalysts were labelled as xNiAl-HP (*x* = 10, 20, 30, 40 and 50, representing the weight percentage of NiO). The catalysts were reduced at 500 °C for 2 h before catalytic reaction (named as R-xNiAl-HP). The 40NiAl-HP catalysts employed in the reaction at 800 °C were named as U-40NiAl-HP-Z (*Z* = 2, 24 and 100, representing the reaction time).

2.1.2 Preparation of Ni-Al₂O₃ by Co-Precipitation

The aqueous solutions of [Ni(NO₃)₂, 0.21 mol/L] and aluminum nitrate [Al(NO₃)₃, 0.47 mol/L] were obtained by dissolving Ni(NO₃)₂·6H₂O and aluminum nitrate nonahydrate [Al(NO₃)₃·9H₂O] in 100 mL of deionized water, respectively. An aqueous solution of NaOH (2 mol/L) was selected as precipitant. The nitrate precursor solution was added to the precipitant solution at a rate of 2 mL/min. The suspension was stirred by a magnetic stirrer and its pH was maintained at about 10. After aging at 70 °C for 12 h, the precipitate was filtered, washed, dried at 100 °C for 12 h and calcined at 450 °C for 2 h under N₂ atmosphere in a tubular furnace (denoted as 40NiAl-CP). The 40NiAl-CP catalyst reduced at 500 °C for 2 h was denoted as R-40NiAl-CP, and the used 40NiAl-CP catalysts at 800 °C were denoted as U-40NiAl-CP-Z (*Z* = 2, 24 and 100, representing the reaction time).

2.2 Catalyst Characterization

The specific surface areas and pore volumes were measured by nitrogen adsorption/desorption at −196 °C on a BeiShiDe 3H-2000PS2 instrument. Before test, the samples were treated under dynamic vacuum at 250 °C for 4 h to remove

the adsorbed impurities. XRD spectra were recorded on a Rigaku D/Max 2500 with a CuK_α X-ray source in a range of 2θ from 10° to 85°. The crystal size of Ni was calculated using the Scherrer–Warren equation [10]. H₂ chemisorption characterization was carried out on a Micrometrics AutoChem II 2920 instrument. Prior to test, 100 mg catalyst was reduced in a H₂ flow at 500 °C for 1 h. Then, the catalysts were purged in Ar at 500 °C for 1 h and cooled down to 30 °C. Finally, pure H₂ was pulsed for 10 min to achieve saturated adsorption. The H₂ capacity and nickel surface area were calculated based on the assumption that one H atom combined with one surface Ni atom and the cross-sectional area of atomic nickel was 6.49 × 10⁻²⁰ m²/Ni-atom [10]. Temperature-programmed reduction of H₂ (H₂-TPR) was carried out on Micrometrics AutoChem II 2920. About 100 mg catalyst loaded in a quartz tube was purged in an Ar flow of 25 mL/min at 300 °C for 30 min and then cooled down to room temperature. The catalyst was heated to 910 °C at a rate of 10 °C·min⁻¹ with a flow of 10 vol% H₂/Ar (20 mL·min⁻¹). X-ray photoelectron spectroscopy (XPS) was conducted on an ESCALab 250Xi electron spectrometer with a non-monochromatized Mg K_α radiation (1253.6 eV). Scanning electron microscopy (SEM) and X-ray energy dispersive spectrometry (EDS) were performed on a JSM-6700F electron microscope. Transmission electron microscopy (TEM) was taken on JEM-2100F at an acceleration voltage of 200 keV.

2.3 Catalyst Evaluation

The CO methanation reaction was performed in a stainless steel fixed bed reactor (Φ20 × 3 × 550 mm) equipped with a quartz tube (Φ12 × 2 × 500 mm, as shown in Fig. S1). Typically, 500 mg catalyst was placed in the constant temperature zone of the reactor, and reduced at 500 °C for 2 h with a gas flow of 50 vol.% H₂/N₂ (30 mL·min⁻¹). The gas mixture of 25 vol.% CO and 75 vol.% H₂ was then introduced to study the catalytic activity at 200–300 °C and catalytic stability at 800 °C. The catalytic experiments were performed at 1.0 MPa with a weight hourly space velocity (WHSV) of 20,000 mL·g⁻¹·h⁻¹. H₂O was removed from the exit gas through a cold trap after reaction for 1 h, and the dry gas entered into an on-line GC-900-SD gas chromatograph equipped with a TCD detector and a 2 m carbon molecular sieve (TDX-1) column. The CO conversion and CH₄ yield were calculated using Eqs. (1) and (2):

CO conversion (X_{co}, %):

$$X_{\text{CO}} = \frac{N_{\text{in}}y_{\text{CO},\text{in}} - N_{\text{out}}y_{\text{CO},\text{out}}}{N_{\text{in}}y_{\text{CO},\text{in}}} \times 100\% \quad (1)$$

CH₄ yield (Y_{CH₄}, %):

$$Y_{\text{CH}_4} = \frac{N_{\text{out}}y_{\text{CH}_4,\text{out}}}{N_{\text{in}}y_{\text{CO},\text{in}} - N_{\text{out}}y_{\text{CO},\text{out}}} \times 100\% \quad (2)$$

where N_{in} or N_{out} denotes as the flow rate (mL·h⁻¹) at the inlet or outlet and y_{in} or y_{out} represents the molar fraction of CO₂ or CH₄ at the inlet or outlet.

3 Results and Discussion

3.1 Catalyst Characterization

3.1.1 Textural Structures of the xNiAl-HP Catalysts with Different Ni Contents

Both the Ni species and crystal structure of the Al₂O₃ support are essential to the catalytic activity of the Ni-Al₂O₃ catalysts [10]. XRD patterns of the as-synthesized and as-reduced catalysts were conducted to determine their crystal structures (Fig. 1). The peaks representing NiO [JCPDS 47–1049, solid line in Fig. 1a], Ni [JCPDS 87–0712, solid line in Fig. 1b], and γ-Al₂O₃ [JCPDS 10–0425, dashed line in Fig. 1a, b] can be observed for the catalysts prepared by hydrolysis-precipitation (xNiAl-HP) [7, 8, 21, 24], suggesting that the γ-Al₂O₃ phase was formed in the xNiAl-HP catalysts during calcination at 450 °C. With increasing nickel content from 10 to 50 wt.%, the diffraction peaks of NiO and Ni become stronger and narrower, while those of γ-Al₂O₃ are weakened gradually, indicating that the crystal sizes of NiO and Ni gradually increase with increasing nickel content. On the other hand, the crystal size of Ni on the xNiAl-HP catalysts, calculated from the width of the Ni (111) diffraction lines using the Scherrer equation, shows an increase from 6.7 to 18.4 nm with increasing nickel content (Table 1).

The Ni2p_{3/2} XPS spectra of the catalysts were detected to verify the nickel species and crystal structure of Al₂O₃ (Fig. 2). The signals at BEs above 855 eV in the xNiAl-HP and 40NiAl-CP catalysts are located between the BEs of NiO (854.1 eV) and NiAl₂O₄ (856.1 eV) with the corresponding shake-up satellite peak (861 eV), further indicating the presence of NiO and NiAl₂O₄ [27, 28]. The binding energy of Ni2p_{3/2} on the xNiAl-HP catalysts is gradually decreased with increasing nickel loading, suggesting that the interaction between nickel and the Al₂O₃ support tends to be weakened. The satellite peak of Ni²⁺ ions can still be observed in all cases, the intensity of which is gradually enhanced with increasing nickel loading, indicating that the xNiAl-HP catalysts with higher nickel content contain more nickel species in the oxidation state [29, 30].

H₂-TPR measurements were carried out to characterize the interaction between the nickel species and the Al₂O₃ support. Based on the peaks in the H₂-TPR spectra (see Fig. 3), the reduced NiO species can be divided into four

Fig. 1 XRD patterns of the xNiAl-HP and 40NiAl-CP catalysts before (a) and after (b) reduction at 500 °C

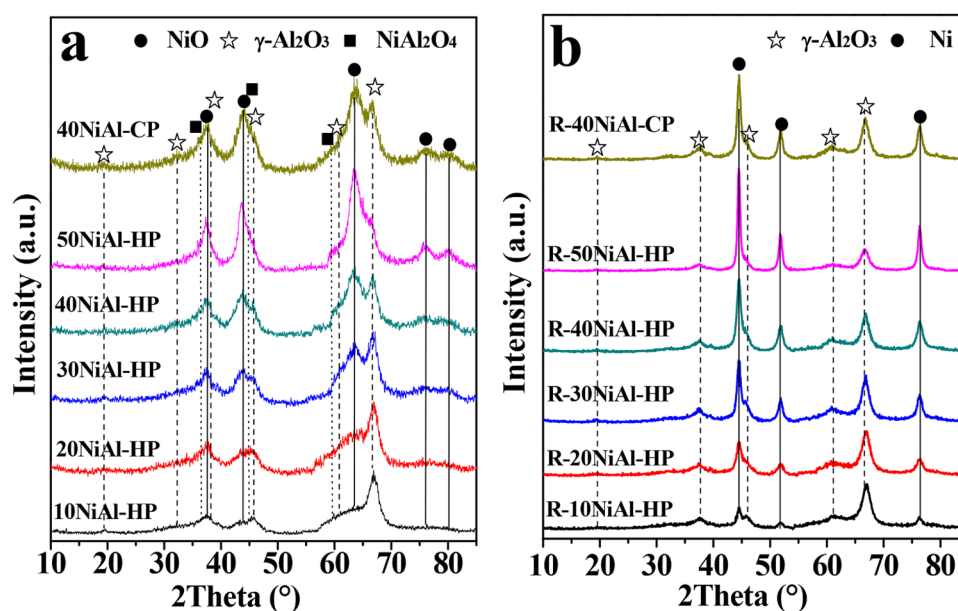


Table 1 Textural properties of the xNiAl-HP and 40NiAl-CP catalysts

Catalyst	Specific surface areas ($\text{m}^2\cdot\text{g}^{-1}$) ^a	Pore volume ($\text{cm}^3\cdot\text{g}^{-1}$) ^b	Pore diameter (nm) ^b	Ni crystallite size (nm) ^c	H ₂ uptake ($\mu\text{mol}\cdot\text{g}^{-1}$) ^d	Ni surface area ($\text{m}^2\cdot\text{g}^{-1}_{\text{cat}}$) ^d
10NiAl-HP	260	0.41	4.4	6.7	36.2	2.8
20NiAl-HP	264	0.42	4.4	8.4	86.6	6.8
30NiAl-HP	277	0.44	4.8	10.2	95.1	7.4
40NiAl-HP	270	0.45	5.2	11.4	225.5	17.6
50NiAl-HP	202	0.60	9.0	18.4	93.8	7.3
40NiAl-CP	257	0.43	4.5	11.8	147.3	11.5

^aThe BET specific surface areas, derived from the BET equation

^bAverage pore volume, obtained from BJH desorption

^cNiO and Ni crystallite size, calculated by the Debye–Scherrer equation

^dDetermined by hydrogen chemisorption

types: α -type in the temperature region lower than 400 °C, β_1 - and β_2 -type in the temperature region of 400–700 °C and γ -type in the temperature region higher than 700 °C [28, 31, 32]. The α -type NiO can be identified as the surface amorphous one that has no and/or weak interaction with the support [21, 31]. The β -type NiO can be classified into Ni-rich mixed oxide phase (β_1) and Al-rich mixed oxide phase (β_2) that possesses a stronger interaction with the support than the former one [21–23, 29, 33]. The γ -type NiO possesses spinel structure (such as NiAl_2O_4) which can strongly interact with the support and cannot be reduced until temperature reaches 700 °C [21–23, 29, 33]. The gaussian fitting analyses of the H₂-TPR patterns of the catalysts are shown in Table S1. Generally, the peak areas of the α - and β -type NiO that represent the content of α - and β -type NiO are increased gradually with increasing nickel content for the NiAl-HP catalysts. Compared with the 40NiAl-CP sample,

the 40NiAl-HP catalyst exhibited the larger amount of α - and β_1 -type NiO species, which is beneficial to the low temperature reactivity [10, 31].

The nickel active surface area is correlated to the number of surface active sites, which can directly affect the catalytic activity [10, 26, 33–35]. The active surface area of Ni species were analyzed via H₂ chemisorption technique [27]. As shown in Table 1, the calculated active surface areas of the xNiAl-HP catalysts follow the order of 40NiAl-HP > 30NiAl-HP > 50NiAl-HP > 20NiAl-HP > 10NiAl-HP, which may induce a higher catalytic activity of 40NiAl-HP.

The physical properties of the Ni-Al₂O₃ catalysts were examined via N₂ adsorption–desorption (see Fig. S2). As shown in Table 1, the BET specific surface areas and pore volumes of the prepared catalysts are in the range of 202–277 m²/g and 0.41–0.60 cm³/g, respectively. The specific surface area of the xNiAl-HP catalysts increased initially with

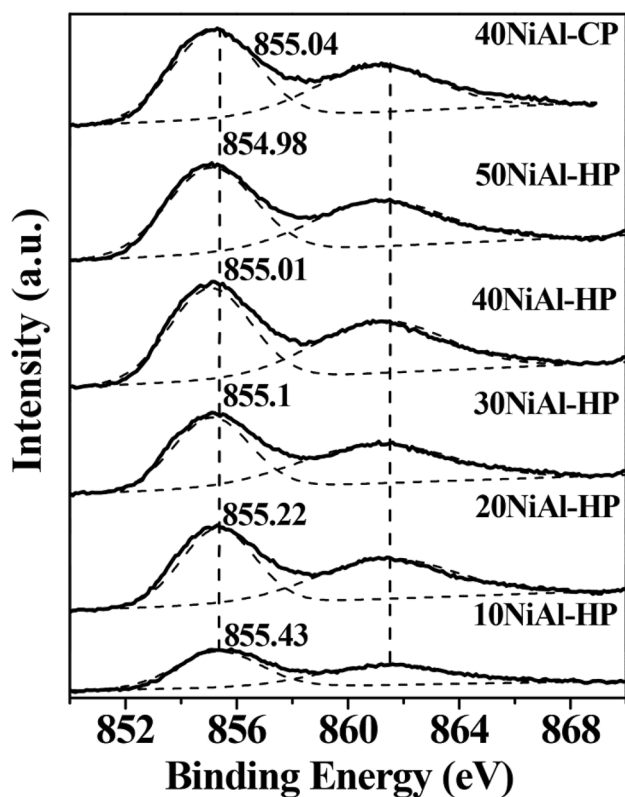


Fig. 2 Ni_{2p_{3/2}} XPS spectra of the xNiAl-HP and 40NiAl-CP catalysts

increasing nickel content and then declined as the nickel loading reaches 50 wt.%, while both the pore volume and average pore size of the catalysts increased throughout. The decreased specific surface area and increased pore size of 50NiAl-HP were probably due to the growth of the catalyst particles.

3.1.2 Structural Comparison of the Catalysts Prepared by Hydrolysis-Precipitation and Co-Precipitation

To gain insight into the effect of preparation method on the textural properties of the Ni-Al₂O₃ catalysts, the textural structures of the catalysts prepared by hydrolysis-precipitation (40NiAl-HP) and co-precipitation (40NiAl-CP) were compared. As shown in Fig. 1, the peaks representing NiO, Ni and γ -Al₂O₃ can also be observed in the XRD pattern of 40NiAl-CP, suggesting a similar texture of 40NiAl-CP with 40NiAl-HP. However, the NiO crystal size on 40NiAl-HP is slightly smaller than that on 40NiAl-CP (Table 1), indicating a better dispersion of NiO on 40NiAl-HP. In the Ni_{2p_{3/2}} XPS spectrum of 40NiAl-CP, the binding energy of NiAl₂O₄ is higher than that of 40NiAl-HP, verifying a larger amount of NiAl₂O₄ spinel on the surface of 40NiAl-CP (see Fig. 2). In the H₂-TPR patterns as shown in Fig. 3, the reduction peaks of α - and β_1 -type NiO on 40NiAl-HP are stronger than

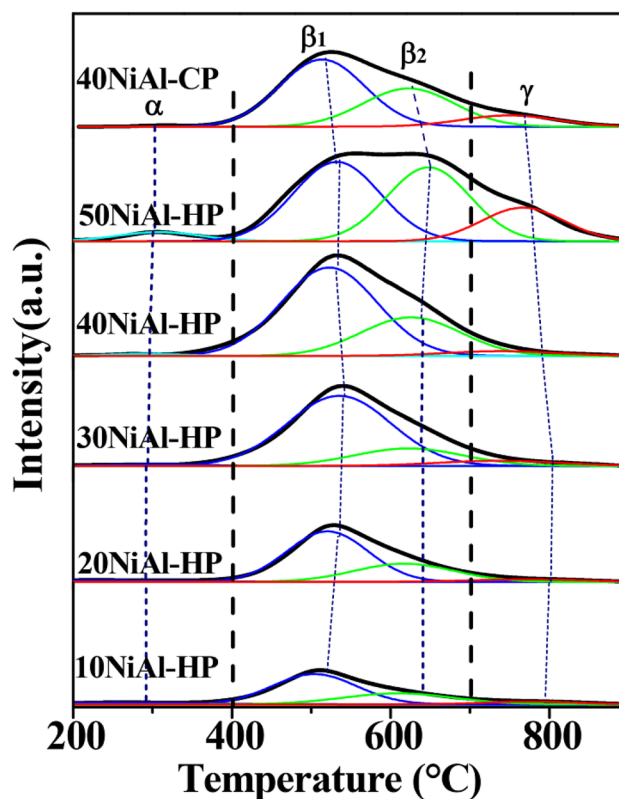


Fig. 3 H₂-TPR profiles of the xNiAl-HP and 40NiAl-CP catalysts

those on 40NiAl-CP, indicating a higher content of α - and β_1 -type NiO on 40NiAl-HP. In addition, as listed in Table 1, the specific surface area, pore volume and pore diameter of 40NiAl-HP are larger than that of 40NiAl-CP, indicating the easy diffusion of reactants and products on 40NiAl-HP in the CO methanation reaction.

TEM and EDS patterns of 40NiAl-CP and 40NiAl-HP were detected to determine the NiO distribution on the catalysts. As shown in Fig. 4, the crystal size of NiO on 40NiAl-CP is *ca.* 4–12 nm with an average size of 6.9 nm, slight larger than that on 40NiAl-HP which is about 3–10 nm with an average size of 5.9 nm. The Ni crystal size, calculated using the Scherrer equation, showed the same trend. The EDS patterns indicated that there was a higher nickel content on the surface of 40NiAl-HP than that of 40NiAl-CP, which would lead to more surface active sites.

It could be concluded that the catalyst prepared by hydrolysis-precipitation (40NiAl-HP) possesses higher specific surface area, better dispersion of NiO, and larger nickel active surface area than that prepared by co-precipitation (40NiAl-CP). To further understand the textural difference of the two catalysts, the mechanisms of hydrolysis-precipitation and co-precipitation were analyzed (see Scheme 1). It was known that pure sodium aluminate was alternatively expressed as NaAlO₂ or NaAl(OH)₄

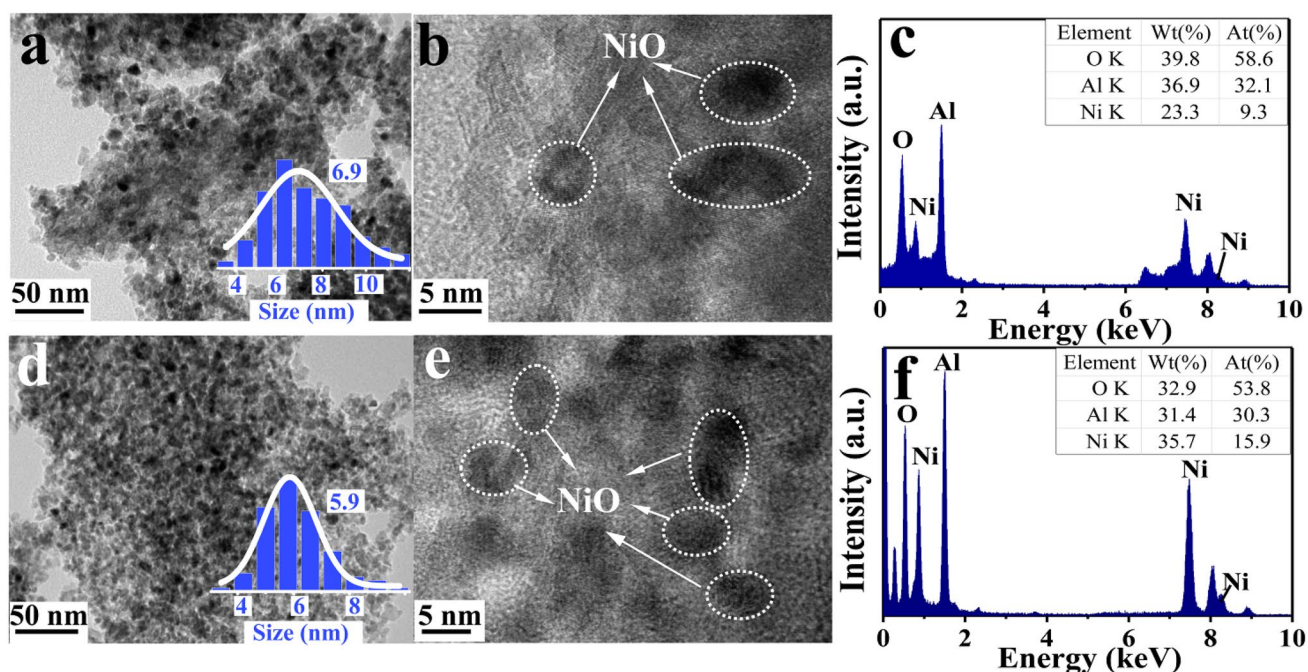
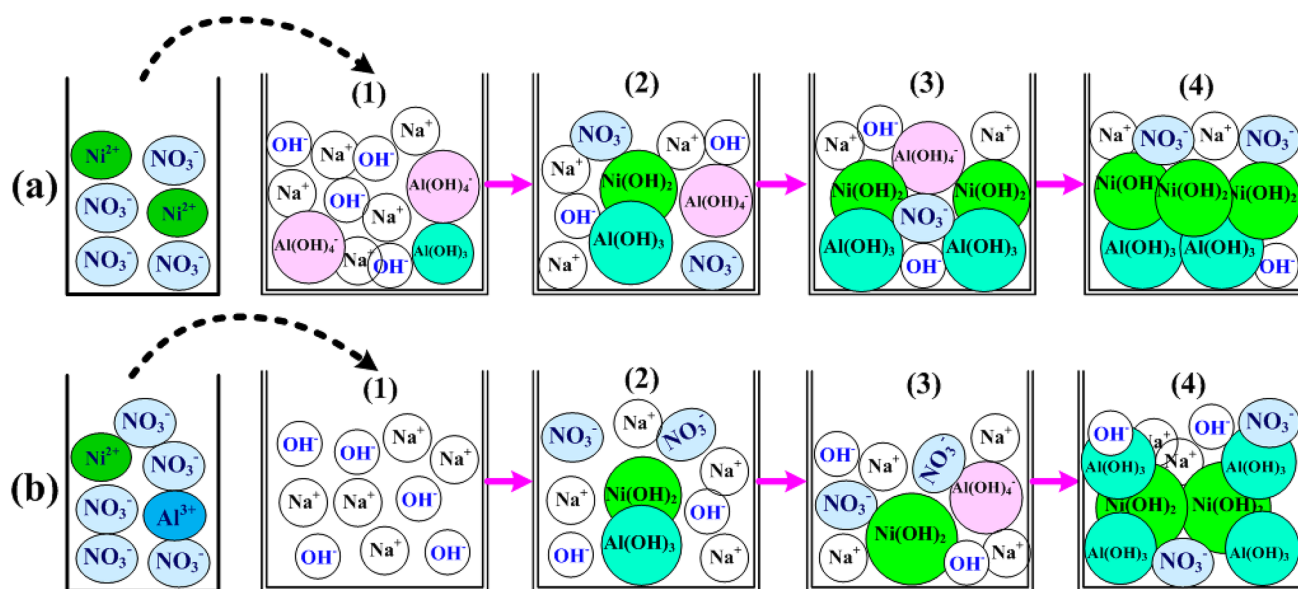
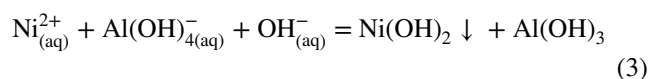


Fig. 4 TEM, size distribution and EDS images of fresh 40NiAl-CP (a–c) and 40NiAl-HP (d–f)



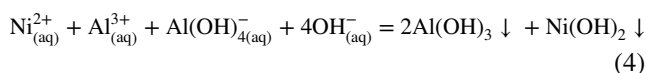
Scheme 1 Schematic models of the hydrolysis-precipitation process (a) and co-precipitation process (b)

(hydrated) [36], and gibbsite and $\text{Al}(\text{OH})_4^-$ are present in the aqueous solution of sodium aluminate [37, 38]. During the hydrolysis-precipitation process, the $\text{Al}(\text{OH})_3$ and $\text{Ni}(\text{OH})_2$ precipitates are simultaneously generated via the reaction between Ni^{2+} and $\text{Al}(\text{OH})_4^-$ [Scheme 1a]. With the continuous addition of $\text{Ni}(\text{NO}_3)_2$, the crystal nuclei of $\text{Al}(\text{OH})_3$ and $\text{Ni}(\text{OH})_2$ gradually grows up. The reaction equation is as follows:



However, the co-precipitation process exhibits different mechanisms [Scheme 1b]. Upon the synchronous addition of the solutions of $\text{Ni}(\text{NO}_3)_2$ and $\text{Al}(\text{NO}_3)_3$ to the NaOH solution, Al^{3+} and Ni^{2+} react quickly with OH^- to produce

Al(OH)₃ and Ni(OH)₂ precipitates. However, Al³⁺ precipitates into Al(OH)₃ in the pH range of 4–10 and exists as D4h-sym-metry Al(OH)₄⁻ in the pH range of 8–12.5 [36–41]. Thus, Al(OH)₃ is rapidly dissolved into Al(OH)₄⁻ in the alkali solution in the early stage of the co-precipitation reaction. With the continuous addition of Ni(NO₃)₂ and Al(NO₃)₃, the crystal nuclei of Ni(OH)₂ continues to grow up and the concentration of Al(OH)₄⁻ keeps rising, followed by decreased pH of the mixed solution. With the rapid consuming of OH⁻, Al(OH)₄⁻ reacts with Al³⁺ to form Al(OH)₃ after the secondary sedimentation. As a result, Al(OH)₃ would be deposited on the surface of Ni(OH)₂ and reduce the nickel active surface area of the catalyst. The reaction equation is as follows:



3.2 Catalytic Performance and Structure-Sensitivity at Low Temperatures

The catalytic performance of the Ni-Al₂O₃ catalysts in CO methanation was assessed at relatively low temperatures (200–300 °C) at 1.0 MPa and WHSV of 20,000 mL/(g·h), and the results are shown in Fig. 5. The catalysts with different nickel loadings were studied; among them, 40NiAl-HP performs optimum activity, which can afford high CO conversion (99%) and CH₄ yield (96%) at a low temperature of 220 °C. The CH₄ yield over the other xNiAl-HP catalysts can reach up to 95% when the reaction temperature is raised to 300 °C.

It is noted that the sequence of the catalytic activity of the xNiAl-HP catalysts follows the order of 40NiAl-HP > 30NiAl-HP > 50NiAl-HP > 20NiAl-HP > 10NiAl-HP, which correlated well with the nickel active surface area (see Table 1). The decrease of CO conversion and CH₄ yield as the nickel loading is increased to 50 wt% should result from the blocking of the external surface of the catalyst by large metal aggregates. It can be concluded that the excellent catalytic activity should be mainly attributed to the high nickel active surface area, which can transform to abundant “exposed” active sites available for the reactants. And just for this reason, the catalytic activity of 40NiAl-HP is higher than that of 40NiAl-CP. Moreover, the activity of Ni-Al₂O₃ catalysts is also consistent with the content of α- and β₁-type NiO species, further indicating that α- and β₁-type NiO play an important role in CO methanation [10, 31].

To evaluate the potential of the Ni-Al₂O₃ catalysts for industrial application, the catalytic performance of 40NiAl-HP was compared with typical reported catalysts (see Table S2). To afford a high catalytic activity, noble metal (Ru), additional promoters (La, B, Zr, CNT, CeO₂) and/or special supports (SiC, Mo₂C, TiO₂) are generally required,

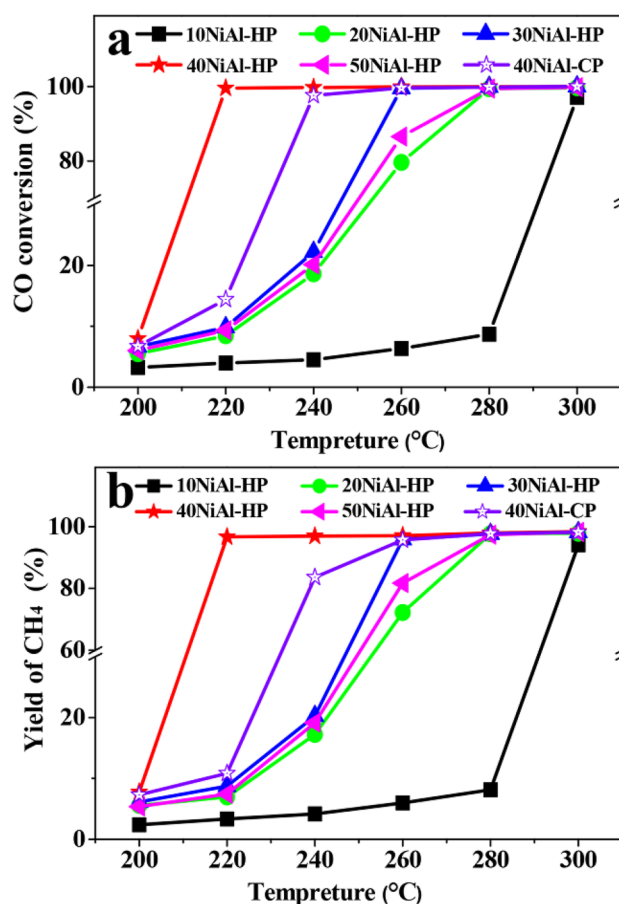


Fig. 5 Effect of reaction temperature on CO conversion (a) and CH₄ yield (b) over different catalysts

which no doubt increase the cost of CO methanation. The 40NiAl-HP catalyst developed in this work exhibits facile preparation method, noble-metal/promoter-free nature, and outstanding catalytic performance at extremely low temperature (220 °C), which would highly reduce the energy consumption and/or operation cost of CO methanation.

3.3 Long-Term Catalytic Stability and Reaction-Sintering at High Temperature

Considering the fact that CO methanation is highly exothermic and the released heat can lead to catalyst deactivation, it is of urgent to detect the catalytic stability of the catalysts under harsh conditions. However, the reaction temperatures and times employed in the literatures (< 600 °C, < 320 h, see Table S3) are generally lower than that commonly adopted in industrial application (650 °C, 1 year) [11]. To reliably reflect the guaranteed lifetime for industrial methanation, a 100 h stability of 40NiAl-HP was tested under the following conditions: H₂/CO=3, T=800 °C, WHSV=20,000 mL/(g·h), P=1.0 MPa. As shown in Fig. 6a, the CO conversion

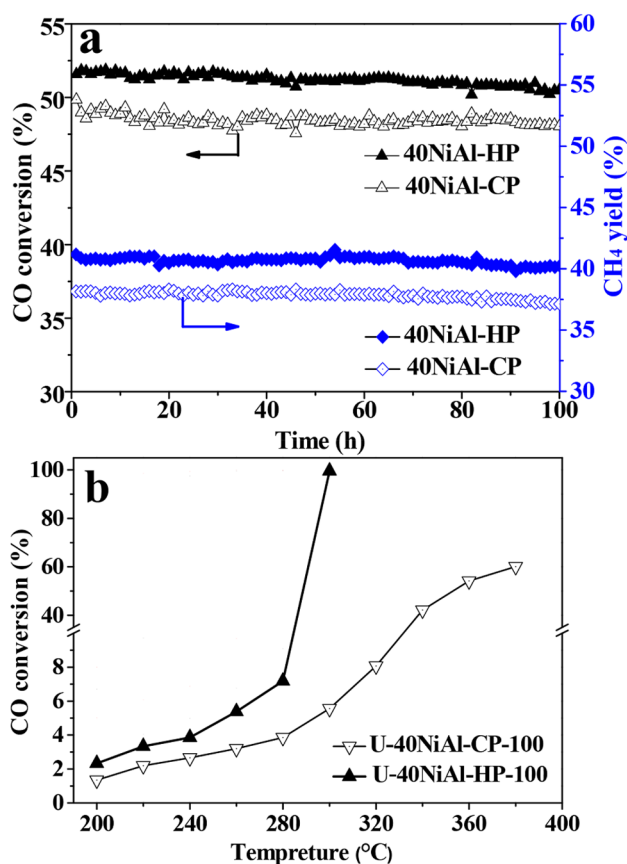


Fig. 6 **a** Catalytic stability of 40NiAl-HP and 40NiAl-CP at high temperature; Reaction conditions: $H_2/CO=3:1$, $WHSV=20,000\text{ mL}\cdot\text{g}^{-1}\cdot\text{h}^{-1}$, $T=800\text{ }^\circ\text{C}$, $P=1.0\text{ MPa}$; **b** Effect of reaction temperature on CO conversion over 40NiAl-HP and 40NiAl-CP after high temperature tests

and CH_4 yield gradually decrease during the entire 100 h on stream, which is probably attributed to the catalyst sintering. Figure 6b showed that the 40NiAl-HP catalyst, previously tested at 800 °C for 100 h, can still afford a CO conversion over 99% at 300 °C, which is satisfactory with the demand of industrial production [42]. However, CO conversion over 40NiAl-CP only reaches 60% at 380 °C and therefore it is inadequate for industrial demand. In conclusion, the 40NiAl-HP catalyst not only showed superior catalytic activity at low temperature but exhibited good stability at high temperature, thereby demonstrating that the catalyst prepared by hydrolysis-precipitation was more suitable for high temperature methanation instead of the conventional one prepared by co-precipitation method.

To gain insight into the sintering process of the 40NiAl-HP and 40NiAl-CP catalysts, their textural properties after being treated at harsh temperatures were analyzed. Figure 7 shows the XRD patterns of the 40NiAl-HP and 40NiAl-CP catalysts post-reacted at 800 °C for different times. The characteristic diffraction peaks of Ni and $\gamma\text{-Al}_2\text{O}_3$ can be clearly

observed on the catalysts as-reduced at 500 °C for 2 h, as shown in Fig. 7a. With increasing reaction time, the diffraction peaks of Ni become stronger, and meanwhile, $\gamma\text{-Al}_2\text{O}_3$ is gradually transformed to θ -type after being used at 800 °C for 24 h [43–46]. After 100 h, a further transformation from θ - to $\alpha\text{-Al}_2\text{O}_3$ occurred on the catalysts [Fig. 7d, [43–45]].

The porous properties of the Ni- Al_2O_3 catalysts treated at 800 °C for different times were examined (Fig. S3). The specific surface area and pore volume of the catalysts declined obviously after being used at 800 °C (see Table 2), which might be explained by the crystal transformation of Al_2O_3 as well as the shrinkage of the catalyst skeleton [47]. Moreover, the specific surface area and pore volume of 40NiAl-HP decline by 82.2% and 36.8% respectively, while those of 40NiAl-CP decline by 86.5% and 41.2% respectively, indicating a rapid sintering speed of 40NiAl-CP than that of 40NiAl-HP.

H_2 chemisorption can further evidence the catalyst sintering. The nickel active surface areas of fresh and spent catalysts as-reduced at 500 °C and post-reacted at 800 °C were determined (see Table 2). For both the 40NiAl-HP and 40NiAl-CP catalysts, a gradual decrease in the nickel active surface area with reaction time can be observed, confirming that sintering could reduce the active sites on catalysts. The active surface areas of 40NiAl-HP and 40NiAl-CP decreased by 94.8% and 97.0% respectively, further indicating the sintering speed of 40NiAl-CP is higher than that of 40NiAl-HP.

SEM images of the 40NiAl-CP and 40NiAl-HP catalysts post-reacted at 800 °C for different times are shown in Fig. 8. One can see that the irregular catalysts gradually migrate, gather and finally evolve to regular spheres with increasing reaction time. For 40NiAl-CP, the average particle size increases from 70.2 to 126.1 nm as the reaction time increased from 2 to 100 h. Under the same condition, the average particle size of 40NiAl-HP increased from 32.8 to 79.2 nm. Meanwhile, the Ni crystal size in the 40NiAl-CP catalyst gradually increases from 11.8 to 68.6 nm at the reaction time of 100 h (see Table 2), which is larger than that in the 40NiAl-HP catalyst (54.5 nm). Based on the analysis of structure characterization, it is revealed that the preparation method had a great effect on the textural structures of the NiAl-based catalyst which is directly related to the catalytic activity.

The sintering mechanism of the Ni- Al_2O_3 catalysts can be deduced (see Scheme 2). The catalyst particles gradually migrate and agglomerate into larger particles with increasing reaction time at 800 °C, leading to the growth of the nickel and alumina crystals. Meanwhile, $\gamma\text{-Al}_2\text{O}_3$ is transformed into θ -type after being used for 24 h. When the reaction time is increased to 100 h, the crystal particles of NiO and Al_2O_3 grow continuously, and $\theta\text{-Al}_2\text{O}_3$ is further transformed to α -type. Both the crystal growth of the catalysts and γ -to- α phase transformation of Al_2O_3 lead to the

Fig. 7 XRD patterns of 40NiAl-HP and 40NiAl-CP as-reduced at 500 °C for 2 h (a) and post-reacted at 800 °C for 2 h (b), 24 h (c) and 100 h (d)

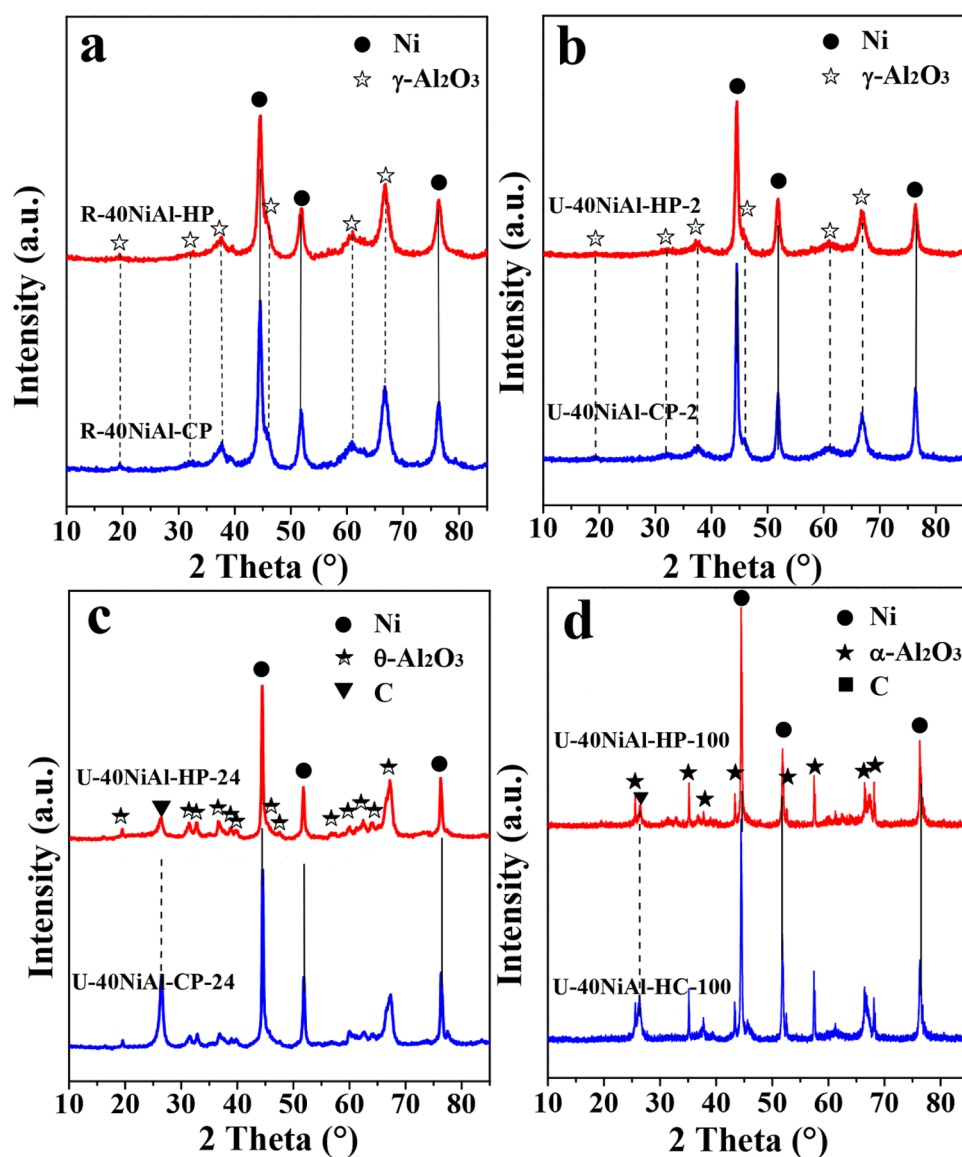


Table 2 Textural properties of 40NiAl-HP and 40NiAl-CP post-treated at high temperatures

Catalyst	Treatment conditions	Specific surface areas (m ² ·g ⁻¹) ^a	Pore volume (cm ³ ·g ⁻¹) ^b	Pore diameter (nm) ^b	Ni crystal size (nm) ^c	H ₂ uptake (μmol·g ⁻¹) ^d	Ni surface area (m ² ·g ⁻¹ _{cat}) ^d
40NiAl-HP	500 °C, 2 h ^e	258	0.38	5.0	11.4	225.5	17.6
	800 °C, 2 h	112	0.36	8.4	17.4	55.4	4.3
	800 °C, 24 h	78	0.32	11.2	25.3	31.3	2.4
	800 °C, 100 h	46	0.24	13.0	54.5	11.7	0.9
40NiAl-CP	500 °C, 2 h ^e	245	0.34	4.5	11.8	147.3	11.5
	800 °C, 2 h	87	0.33	10.9	22.4	33.5	2.6
	800 °C, 24 h	62	0.26	11.4	31.8	13.4	1.1
	800 °C, 100 h	33	0.20	16.9	68.6	4.4	0.4

^aSpecific surface areas are derived from the BET equation; ^bObtained from BJH desorption average pore volume; ^cNiO and Ni crystallite size, calculated by the Debye–Scherrer equation; ^dDetermined by hydrogen chemisorption. ^eReduced at 500 °C for 2 h

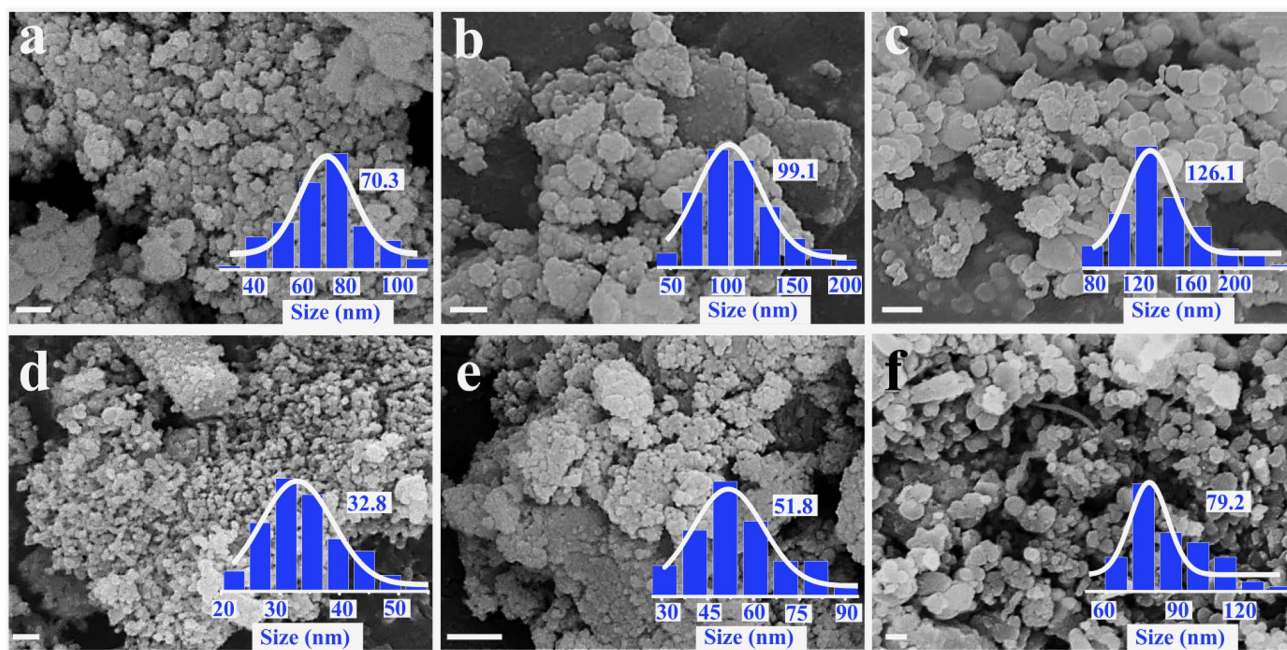


Fig. 8 SEM and particle distribution images of **a** U-40NiAl-CP-2, **b** U-40NiAl-CP-24, **c** U-40NiAl-CP-100, **d** U-40NiAl-HP-2, **e** U-40NiAl-HP-24, and **f** U-40NiAl-HP-100. Scale bars in SEM images: 200 nm

significant decrease of the specific surface area and active surface area, by which the catalytic activity at low temperature declines.

4 Conclusions

A series of Ni- Al_2O_3 catalysts have been prepared via hydrolysis-precipitation for CO methanation, and the effect of the textural structures on catalytic activity at low temperature and long-term catalytic stability at high temperature has been established. Herein, 40NiAl-HP catalyst exhibits optimal activity at low temperature (220 °C), which can catalyze CO into CH_4 with excellent CO conversion (99%) and CH_4 yield (96%). The high content of α - and β_1 -type NiO, good dispersion of NiO, and high nickel active surface area are responsible for the superior catalytic activity of 40NiAl-HP. The sintering of the catalysts at 800 °C induces

the migration and growth of NiO crystallites, the γ -to- θ -to- α phase transformation of Al_2O_3 , and the diffusion and agglomeration of the catalysts. A 99% of CO conversion can still be achieved over 40NiAl-HP at 300 °C after being used at 800 °C for 100 h, making it a competitive candidate for industrial methanation.

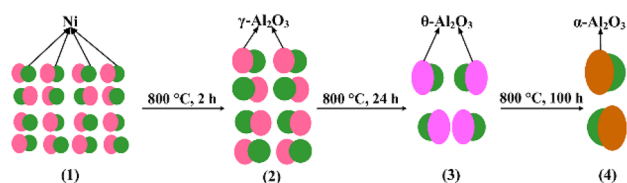
Acknowledgements This work was supported by the Technology Innovation Project for Excellent Talents of Shanxi Province (No. 201805D211037), Coal Based Key Scientific and Technological Project of Shanxi Province (No. MJH2016-03).

Compliance with Ethical Standards

Conflict of interest The authors declare that they have no conflict of interest.

References

- International energy outlook 2011 <http://www.eia.gov/R>.
- Razzaq R, Li CS, Zhang SJ (2013) Fuel 113:287
- Cao WS, Bluth C (2013) Energy Policy 53:381
- Shi Y, Xia Y, Lu B, Liu N, Zhang L, Li S, Li W (2014) J Zhejiang Univ-Sci A (Appl Phys Eng) 15:454
- Kang Z (2014) Nat Gas Industry B 1:103–112
- Li J, Wang H, Zhu QS, Li HZ (2019) Chem Eng J 357:298
- Wang H, Xu K, Yao XY, Ye DH, Pei Y, Hu HR, Qiao MH, Li ZH, Zhang XX, Zong BN (2018) ACS Catal 8:1207
- Man Y, Han YL, Hu YS, Yang S, Yang SY (2018) J Clean Prod 172:2503



Scheme 2 Schematic model of the reaction-sintering process of the Ni- Al_2O_3 catalysts at 800 °C

9. Liu Q, Gu FN, Lu XP, Liu YJ, Li HF, Zhong ZY, Xu GW, Su FB (2014) *Appl Catal A* 488:37
10. Qin ZF, Ren J, Miao MQ, Li Z, Lin JY, Xie KC (2015) *Appl Catal B Environ* 164:18
11. Nguyen TTM, Wissing L, Skjøth-Rasmussen MS (2013) *Catal Today* 215:233
12. Ren J, Li HD, Jin YY, Zhu JY, Liu SS, Lin JY, Li Z (2017) *Appl Catal B Environ* 201:561
13. Muñoz-Murillo A, Martínez LM, Domínguez MI, Odriozola JA, Centeno MA (2018) *Appl Catal B Environ* 236:420
14. Bobadilla LF, Muñoz-Murillo A, Laguna OH, Centeno MA, Odriozola JA (2019) *Chem Eng J* 357:248
15. Meng FH, Li X, Shaw G, Smith PJ, Morgan DJ, Perdjon M, Li Z (2018) *Ind Eng Chem Res* 57:4798
16. Meng FH, Li X, Li MH, Cui XX, Li Z (2017) *Chem Eng J* 313:1548
17. Le TA, Kim T, Lee SH, Park ED (2018) *Catal Today* 303:159
18. Li J, Zhou L, Li PC, Zhu QS, Gao JJ, Gu FN, Su FB (2013) *Chem Eng J* 219:183
19. Gao JJ, Jia CM, Li J, Zhang MJ, Gu FN, Xu GW, Zhong ZY, Su FB (2013) *J Energy Chem* 22:919
20. Olesen SE, Andersson K, Damsgaard CD, Chorkendorff I (2017) *J Phys Chem C* 121:15556
21. Zhao AM, Ying WY, Zhang HT, Ma HF, Fang DY (2012) *Catal Commun* 17:34
22. Ma SL, Tan YS, Han YZ (2011) *J Nat Gas Chem* 4:435
23. Fan MT, Miao KP, Lin JD, Zhang HB, Liao DW (2014) *Appl Surf Sci* 307:682
24. Cheng CB, Shen DK, Xiao R, Wu CF (2017) *Fuel* 189:419
25. Yan Y, Dai YH, He H, Yu YB, Yang YH (2016) *Appl Catal B Environ* 196:108
26. Rostrup-Nielsen JR, Pedersen K, Sehested J (2007) *Appl Catal A* 330:134
27. Koschany F, Schlereth D, Hinrichsen O (2016) *Appl Catal B Environ* 181:504
28. Yang RC, Wu JS, Li XG, Zhang X, Zhang ZH, Guo JT (2012) *Appl Catal A* 383:112
29. Wang R, Li YH, Shi HR, Yang MM (2011) *J Mol Catal A Chem* 344:122
30. Abelló S, Verboekend D, Bridier B, Pérez-Ramírez (2008) *J Catal* 259:85
31. Seo YS, Jung YS, Yoon WL, Jang IG, Lee TW (2011) *Int J Hydrogen Energy* 36:94
32. Zhang JF, Bai YX, Zhang QD, Wang XX, Zhang T, Tan YS, Han YZ (2014) *Fuel* 132:211
33. Aziz M, Jalil AA, Triwahyono S, Mukti RR, Taufiq-Yap YH, Sazegar MR (2014) *Appl Catal B Environ* 147:359
34. Dai XP, Liang J, Ma D, Zhang X, Zhao HB, Zhao B, Guo ZG, Kleitz F, Qiao S (2015) *Appl Catal B Environ* 165:752
35. Chen JL, Ma Q, Rufford TE, Li YD, Zhu ZH (2009) *Appl Catal A* 362:1
36. Tian DY, Liu ZH, Li DD, Shi HL, Pan WX, Cheng Y (2013) *Fuel* 104:224
37. Lebarbier VM, Dagle RA, Kovarik L, Albrecht KO, Li XH, Li LY, Taylor CE, Bao X, Wang Y (2014) *Appl Catal B Environ* 144:223
38. Shaaban A, Hayashi S, Azumi K (2017) *Surf Coat Tech* 325:673
39. Pantias D, Asimidis P, Paspaliaris I (2001) *Hydrometallurgy* 59:15
40. Skoufadis C, Pantias D, Paspaliaris I (2003) *Hydrometallurgy* 68:57
41. Surhone LM, Tennoe MT, Henssonow SF (2010) *Sodium aluminate*. Betascript publishing
42. Alihosseinzadeh A, Nematollahi B, Rezaei M, Lay EN (2015) *Int J Hydrogen Energy* 40:1809
43. Nguefack M, Popa AF, Rossignol S, Kappenstein C (2003) *Phys Chem Chem Phys* 5:4279
44. Carreira LA, Maroni VA, Swaine JW Jr, Plumb RC (1966) *J Chem Phys* 45:2216
45. Baes F, Mesmer RE (1977) *Science* 4284:1323–1324
46. Naykki T, Raimo A, Paavo P, Antero K, Paivi N (2000) *Talanta* 52:755
47. Zhu H (2002) *Preparation and applied technology of catalyst support*. Petroleum industry press, Beijing

Publisher's Note Springer Nature remains neutral with regard to jurisdictional claims in published maps and institutional affiliations.

Affiliations

Zhifeng Qin^{1,4,5} · Hongyan Ban¹ · Xiaoyue Wang¹ · Zhibin Wang¹ · Yanxia Niu² · Ying Yao³ · Jun Ren¹ · Liping Chang¹ · Maoqian Miao¹ · Kechang Xie¹ · Congming Li¹

¹ Key Laboratory of Coal Science and Technology, Ministry of Education and Shanxi Province, Taiyuan University of Technology, Taiyuan 030024, China

² School of Chemistry and Chemical Engineering, Taiyuan University of Technology, Taiyuan 030024, China

³ Department of Chemistry and Chemical Engineering, Taiyuan Institute of Technology, Taiyuan 030008, China

⁴ Post-Doctoral Research Station of Shanxi Institute of Environmental Planning, Taiyuan 030002, China

⁵ Postdoctoral Mobile Station of Environmental Science and Engineering, Tsinghua University, Beijing 100084, China